Journal of Materials Chemistry C

ROYAL SOCIETY OF CHEMISTRY

PAPER

View Article Online
View Journal | View Issue

Cite this: J. Mater. Chem. C, 2024, 12, 2903

Self-assembled D–π–A multifunctional systems with tunable stimuli-responsive emission and optical waveguiding behaviour†

R. Martín,‡[ab] A. Sánchez-Oliva,‡[b] A. Benito,[a] I. Torres-Moya,[bc] A. M. Garcia,[b] J. Álvarez-Conde,[d] J. Cabanillas-González,*[d] P. Prieto*[b] and B. Gómez-Lor*[a]

Received 8th November 2023,
Accepted 16th January 2024

DOI: 10.1039/d3tc04100j

rsc.li/materials-c

Smart materials with stimuli-responsiveness are a subject of great attention nowadays. In this work, we describe two D–π–A naphthalenimide (NI) derivatives, with different *N*-functionalization prepared by an environmentally benign process. They self-assemble into fluorescent crystals that display optical waveguiding behaviour with low optical loss coefficients. In addition, they present thermal/mechanical stimuli-responsiveness, which is tuned upon substitution at the molecular main core as a result of changes in crystal packing. A cold-crystallization process, as confirmed by DSC and power X-ray analysis, was identified as the underlying cause of the colour change upon heating, which can be reverted due to an amorphization process upon shearing. The combination of the reversible coloured amorphous-crystalline phase transition, together with the light guiding, holds significant promise for practical applications including use in security inks, rewritable materials or modern optics.

Introduction

Optoelectronic devices play an essential role in modern technology, enabling a wide range of applications in various fields. In this technology, light confinement and light in- or out-coupling is important for the development of lasers, optical amplifiers or photodetectors.[1,2]

Organic crystals possess interesting features for optoelectronic applications in comparison with their inorganic counterparts.[3] They are lighter, present different morphologies and very importantly, their properties can be tuned at the molecular level thanks to the opportunities offered by organic synthesis.[4] Focusing on their emissive properties, some organic crystals combine high fluorescence quantum yields with notable light waveguiding properties, arising from low optical losses and refractive indexes in the 1.8–2.2 range, and a good photoluminescence efficiency. Up to now, a great number of organic crystals with excellent performance as optical waveguiding materials have been reported,[5–7] although recently, additional features have been put into play. This implies the development of more complex materials as doped structures,[8] core/shell structures[9] or heterostructures,[10] and the incorporation of features such as flexibility,[11–13] anisotropy,[14] chiral elements[15] or stimuli-responsiveness.[16,17]

The combination in a single material of optical waveguiding properties and stimuli-responsiveness arouses much interest due to the potential applications in the optoelectronics and sensors fields. In this sense, Yawen *et al.* described five cyano-functionalized 1,4-bis((*E*)-2-(1*H*-indol-3-yl)vinyl)benzene derivatives, substituted with alkyl chains of variable length. Interestingly, while compounds with short side chains displayed optical waveguiding properties, those with long ones showed thermochromism.[18] In another example, Jia and coworkers reported a single organic crystal of a derivative that connects a pyrene unit and a rhodamine B moiety through a CN group. This crystal possessed multiple properties including optical waveguiding and mechanochromism.[19]

The use of physical stimulation, such as pressure or temperature, to induce changes in the absorption or emission spectra[20,21] arouses much interest to develop tuneable optoelectronic devices. These types of switchable material are attractive candidates in fields as varied as sensors,[22] recording

[a] Institute of Materials Science of Madrid (ICMM-CSIC), Sor Juana Inés de la Cruz 3, Cantoblanco 28049, Madrid, Spain. E-mail: bgl@icmm.csic.es
[b] Faculty of Chemical Science and Technology, University of Castilla-La Mancha, Instituto Regional de Investigación Científica Aplicada (IRICA), University of Castilla-La Mancha, 13071 Ciudad Real, Spain. E-mail: Mariapilar.Prieto@uclm.es
[c] Department of Organic Chemistry, Faculty of Chemical Sciences, Campus of Espinardo, University of Murcia, 30100 Murcia, Spain
[d] Madrid Institute for Advanced Studies, IMDEA Nanociencia, Calle Faraday 9, Cantoblanco, 28049, Madrid, Spain. E-mail: juan.cabanillas@imdea.org

† Electronic supplementary information (ESI) available. CCDC 2306088 and 2306089. For ESI and crystallographic data in CIF or other electronic format see DOI: https://doi.org/10.1039/d3tc04100j

‡ These authors contributed equally to this work.

technologies,[23] security inks[24] or rewritable paper.[25] The extent of the colour changes can vary, ranging from subtle changes to complete colour loss/gain in response to stimuli-induced modifications on molecular conformation, intermolecular interactions, and crystal packing.[26–30] A combination of both types of stimulation, *i.e.*, preparation of organic crystals able to offer a response to both mechanical and thermal stimuli in different directions, is even more interesting in the quest for multi-responsive, smart materials.[31,32]

Although in the last few years impressive advances have been achieved in the development of crystalline organic waveguides and stimuli responsive materials, more detailed studies are required to advance the *ad hoc* design of smart materials with desired functions, whereby optical properties and response to stimuli are rationalized from the chemical structure of the molecules. Bearing this in mind, we here report a study of two D–π–A systems featuring a triphenylamine derivative joined to two differently substituted 1,8-naphthalimide (NI) acceptors *via* an ethynyl bridge. Both derivatives lead to the formation of multifunctional structures that exhibit thermochromism, mechanochromism and optical waveguide behaviour. The response to various stimuli depends on the specific substitution of the NI core present in the molecules. Additionally, XRD analysis aids to establish a correlation between the observed structural features and the mechanochromic and waveguiding behaviour.

Experimental

Synthesis of NI derivatives

Synthesis of 2-(3,5-bis(trifluoromethyl)phenyl)-6-bromo-1,8-naphthalimide (2a)[33]. A mixture of 4-bromo-1,8-naphthalic anhydride (0.100 g, 0.361 mmol) with 3,5-bis(trifluoromethyl)aniline (0.124 g, 0.542 mmol) and zinc acetate dihydrate (0.126 g, 0.578 mmol) was added under argon to a dried microwave vessel. Then, 1 mL of quinoline was added. After that, the vessel was closed and irradiated at 150 °C for 60 min. The obtained crude reaction product was washed with 1 M HCl and the organic phase was extracted with three portions of 10 mL of CH_2Cl_2. The organic phase was dried over $MgSO_4$ and the solvent evaporated under vacuum. Finally, the obtained solid was washed with ethanol and dried under vacuum to give compound **2a** as a white solid (166 mg, 94%).

^{1}H-NMR ($CDCl_3$, 500 MHz) (δ, ppm): 8.73 (d, J = 7.9 Hz, 1H, H_{NI}), 8.71 (d, 1H, J = 7.8 Hz, H_{NI}), 8.49 (d, 1H, J = 7.9 Hz, H_{NI}), 8.14 (d, 1H, J = 7.9 Hz, H_{NI}), 8.00 (s, 1H, H*p*-phenyl), 7.93 (t, 1H, J = 7.9 Hz, H_{NI}), 7.83 (s, 2H, H*o*-phenyl).

Synthesis of 6-bromo-2-octyl-1,8-naphthalimide (2b)[34]. A mixture of 4-bromo-1,8-naphthalic anhydride (0.100 g, 0.361 mmol) with octylamine (0.047 g, 0.361 mmol) was added under argon to a dried microwave vessel. Then, 0.5 mL of ethanol was added. After that, the vessel was closed and irradiated at 80 °C for 30 min. The obtained crude reaction product was washed with ethanol and dried to give compound **2b** as a white solid (133 mg, 95%).

^{1}H-NMR ($CDCl_3$, 500 MHz) (δ, ppm): 8.67 (d, J = 7.8 Hz, 1H, H_{NI}), 8.58 (d, 1H, J = 7.8 Hz, H_{NI}), 8.42 (d, 1H, J = 7.8 Hz, H_{NI}), 8.05 (d, 1H, J = 7.8 Hz, H_{NI}), 7.85 (t, 1H, J = 7.8 Hz, H_{NI}), 4.16 (t, 2H, J = 6.6 Hz, N–CH_2–), 1.73 (m, 2H, –CH_2–), 1.40 (m, 2H, –CH_2–), 1.35 (m, 2H, –CH_2–), 1.29 (m, 6H, –CH_2–), 0.87 (t, 3H, –CH_3).

Synthesis of 6-((4-(diphenylamino)phenyl)ethynyl)-2-(3,5-bis(trifluoromethyl)phenyl)-1,8-naphthalimide (NI1). A mixture of 2-(3,5-bis(trifluoromethyl)phenyl)-6-bromo-1,8-naphthalimide (0.100 g, 0.205 mmol) with 4-ethynyl-*N*,*N*-diphenylaniline (0.069 g, 0.256 mmol), DBU (0.062 g, 0.411 mmol), CuI (0.002 g, 0.010 mmol) and Pd-EncatTM TPP30 (0.018 g, 0.007 mmol) was prepared under argon in a dried microwave vessel. Then, 1 mL of CH_3CN was added. After that, the vessel was closed and irradiated at 130 °C for 20 min. The obtained crude reaction product was purified by column chromatography, using hexane/ethyl acetate (9/1) as eluents to give compound **NI1** as a bright orange solid (88 mg, 63%).

M.p.: 239–240 °C. ^{1}H-NMR ($CDCl_3$, 500 MHz) (δ, ppm): 8.88 (d, J = 8.4 Hz, 1H, H_{NI}), 8.73 (d, 1H, J = 8.4 Hz, H_{NI}), 8.64 (d, 1H, J = 8.4 Hz, H_{NI}), 8.02 (s, 1H, *p*-Ph-CF3), 7.99 (d, 1H, J = 8.4 Hz, H_{NI}), 7.92 (t, 1H, J = 8.4 Hz, H_{NI}), 7.86 (s, 2H, *o*-Ph-CF3), 7.54 (d, 2H, J = 8.8 Hz, *m*-N-PhC-≡), 7.35 (t, 4H, *m*-N-Ph), 7.19 (d, 2H, J = 8.8 Hz *o*-N-PhC-≡), 7.18 (d, 4H, J = 8.8 Hz, *o*-N-Ph), 7.13 (t, 2H, J = 8.8 Hz, *p*-N-Ph). ^{13}C-NMR (δ, ppm): 164.1, 163.8, 148.9, 147.1, 143.0, 136.9, 135.8, 132.8, 132.6, 132.0, 131.1, 129.9, 129.5, 128.2, 126.8, 125.1, 124.0, 123.5, 120.8, 120.2, 100.0. MS (MALDI TOF/TOF, m/z) 676.463, required for $C_{40}H_{22}F_6N_2O_2$, 676.159.

Crystallization of NI derivatives

NI1 and **NI2** crystals were obtained employing the slow diffusion technique. Briefly, a vial with 1 mL of a 1 mg/mL solution in THF of the corresponding NI derivative was introduced into a bigger vial, containing 3 mL of the poor solvent, hexane and methanol for **NI1** and **NI2**, respectively. The whole system was closed, and crystals appeared after a period of 1–2 weeks.

Results and discussion

Design, synthesis and characterization of the molecules

The NI core was selected in view of its acceptor character and its easy chemical modulation to build D–π–A conjugated systems, as well as for its ability to form fluorescent supramolecular aggregates.[35–37] On the other hand, the triphenylamine group is a good donor that favours red-shifting and contributes to a good packing,[38] while the triple bond enables the formation of good crystal structures thanks to the existence of CH–π interactions.[39] The *N*-substitution of the naphthalimide group with either a diCF_3-phenyl group (**NI1**) or an alkyl chain (**NI2**) has a profound impact on self-assembly and packing, and therefore on the properties of the supramolecular materials obtained.

The synthesis of compound **NI2** has been previously reported by some of the authors,[34] while compound **NI1** was synthesized for the first time in this work, following a similar

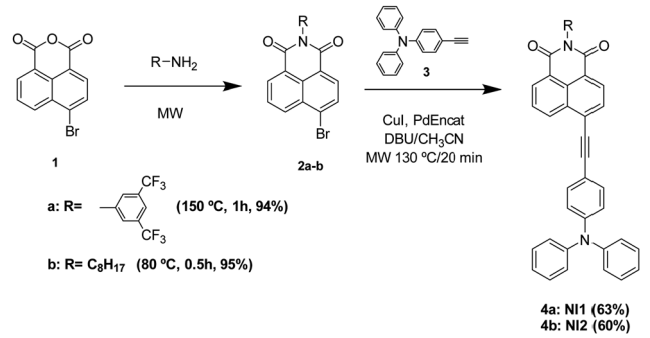

Scheme 1 Synthesis of D–π–A NI derivatives.

procedure that involves a two-step process according to the principles of sustainable chemistry.[40,41] First, the imide was formed using 4-bromo-1,8-naphthalic anhydride and the corresponding amine followed by a Sonogashira coupling reaction with the alkynyl donor fragment.[34] Microwave radiation was used as the energy source, which results in a significant decrease in reaction time and a large increase in yield, and it is carried out with a minimum amount of solvent and using a reusable catalyst (Pd-Encat TPP30) (Scheme 1, see ESI,† Section S2 for NMR and MS details).

Spectroscopic measurements (UV-vis, fluorescence)

The absorption and photoluminescence (PL) spectra of NI derivatives in solution were recorded in $CHCl_3$ at a concentration of 10^{-5} M upon photoexciting the samples at the absorption maxima of the lowest energy band. The most relevant data are summarized in Fig. 1 and Table 1.

The absorption spectra of both NI derivatives in $CHCl_3$ are similar except for a slight redshift of **NI1** with respect to **NI2**. They are characterized by a band centred at 330–350 nm, which corresponds to a π–π* transition, and another band at longer wavelength (lower energy) that it is indicative of an ICT process from the triphenylamine donor to the NI acceptor core. The presence of two $-CF_3$ groups in the **NI1** groups enhances the electron scavenging nature of the NI core, increases the ICT character of this derivative and gives rise to a bathochromic

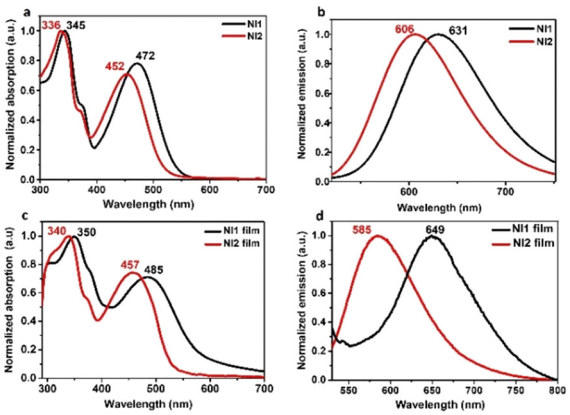

Fig. 1 Absorption and emission spectra of the NI compound solution ($CHCl_3$, 1×10^{-5} M) (a) and (b) and in thin films (c) and (d).

Table 1 Photophysical data for NI derivatives

	Solution				Films	
Compound	λ_{abs}[a] (nm)	ε (M^{-1} cm^{-1}) $\times 10^4$ [b]	λ_{em}[c] (nm)	ϕ[d]	λ_{abs}[e] (nm)	λ_{em}[f] (nm)
NI1	345/472	3.3/2.7	631	0.95	350/485	649
NI2	336/452	3.1/2.4	606	0.94	340/457	585

[a] Maximum absorption wavelengths measured in 10^{-5} M $CHCl_3$ solution. [b] ε stands for molar extinction coefficient at the first and second λ_{abs} values, respectively. [c] Maximum emission wavelength measured in 10^{-5} M $CHCl_3$ solution (λ_{exc} (**NI1**) = 472 nm and λ_{exc} (**NI2**) = 452 nm). [d] PL quantum yield measured in $CHCl_3$ using cresyl violet in ethanol (Φ = 0.56) for **NI1** and quinine sulphate in 0.1 M H_2SO_4 (Φ = 0.54) and fluorescein in 0.1 M NaOH (Φ = 0.79) for **NI2**. [e] Maximum absorption wavelengths measured in the film. [f] Maximum emission wavelengths measured in the film (λ_{exc} (**NI1**) = 485 nm and λ_{exc} (**NI2**) = 457 nm).

shift (Fig. 1a). A similar trend can be observed in the fluorescence spectra in solution, with the maximum emission wavelength of **NI1** red-shifted compared to **NI2** (631 *vs.* 606 nm) (Fig. 1b), when excited at the ICT band (note that excitation at the π–π* energy band does not produce changes in the emission wavelengths, see Fig. S9, ESI†). Remarkably, both compounds exhibited highly emissive properties in solution, with fluorescence quantum yields of 0.94 and 0.95 for **NI1** and **NI2**, respectively (Table 1).

The absorption spectra of the two compounds in the film resemble those in solution (Fig. 1c), but important differences emerge from the fluorescence spectra (Fig. 1d). Whereas the introduction of $-CF_3$ groups at the NI core (**NI1**) leads to a slight bathochromic shift in the solid state with respect to solution (649 *vs.* 631 nm) ascribed to a change in the dielectric medium, the emission spectra of **NI2** films are significantly blue shifted compared to solution (585 *vs.* 606 nm). These differences in solid state fluorescence denote a likely change in crystal packing modulated by the side substituents, as will be demonstrated (vide infra). Curiously, when comparing the fluorescence spectra of solutions and films, **NI1** shows a notable redshift, indicating a strong electronic coupling of the constituent molecular units. Conversely, the emission spectra of **NI2** films are blue shifted when compared to its solution state. Probably, in this particular case, the steric hindrance introduced by the flexible alkyl chains impedes the emergence of close π-interactions between molecules in the solid state, which would favour the electronic delocalization.

Optical waveguide properties of NI crystals

Crystals from the reported D–π–A 1,8-naphthalimides were obtained using the slow diffusion technique (see Experimental).

NI1 showed needle-like crystals between 0.5-1 mm length, appropriate for the study of the optical waveguiding behaviour, when THF is used as a good solvent and hexane as a poor solvent (Fig. S6, ESI†). On the other hand, **NI2** formed rectangular slabs appropriate for optical waveguiding studies in THF as a good solvent and methanol as a poor solvent, although they are slightly smaller than the ones for **NI1** (Fig. S7, ESI†).

PL microscopy images and spectra were recorded for crystals of NI derivatives to qualitatively evaluate their optical waveguiding

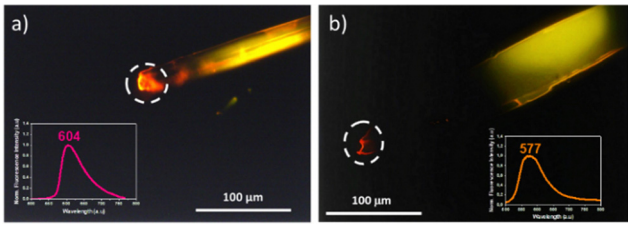

Fig. 2 PL microscopy images and emission spectra for the single crystals of (a) **NI1** and (b) **NI2**.

behaviour (Fig. 2). Both microscopy images depict bright orange fluorescence from crystals of both NI compounds upon photoexcitation at 355 nm as well as emission from the tips, although slightly weaker than from the bulk, evidencing active optical waveguiding capability.

In addition, in order to evaluate the efficiency of the optical waveguides obtained from NI crystals, the optical loss coefficients were measured upon moving the photoexcitation (355 nm) spot along the length of the crystal while detecting the emission at one of the tips (Fig. 3a). A schematic representation of the set-up used for the measurements can be found in Fig. S8 (ESI†). The fluorescence intensity (I_{out}) upon moving the pump a distance x with respect to the initial position (I_{in}) is given by the Lambert–Beer law $I_{out} = I_{in}e^{-\alpha x}$, where I_{out} and I_{in} are the PL intensities at the output and input, respectively, x is the propagation distance, and α is the absorption coefficient in μm^{-1}, which is related to the optical loss coefficient α' (dB μm^{-1}) through the equation α' (dB μm^{-1}) $\approx 4.34\alpha$ (μm^{-1}). The α and α' values obtained for **NI1** were 2.1×10^{-3} μm^{-1} and 9.1×10^{-3} dB μm^{-1}, respectively (Fig. 3b). The α' value is lower than some recently reported in optical waveguiding organic crystals[42–44] and on the order of the best derivatives reported recently by our research group[45] and by others.[46] It is known that the excellent crystallinity improves the exciton-photon coupling and the migration of excitons, favouring the light transmission process.[47] In the case of **NI2**, it was not possible to determine the α' value because the crystals obtained were not large enough to be studied with our experimental setup.

The outcomes indicate that the presence of diCF_3-phenyl substituents contributes to the formation of better quality and larger crystals when compared to the alkyl chains.

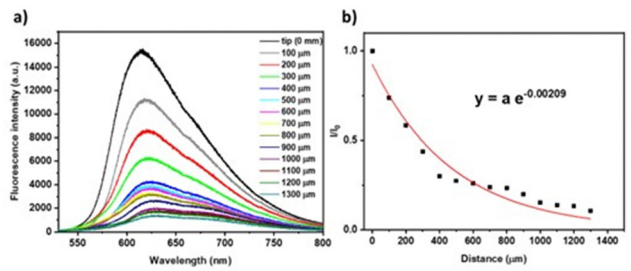

Fig. 3 (a) PL spectra of the crystals collected at the end tip upon varying the distances between the excitation and the tip of **NI1**. (b) Ratio between the PL intensities photoexcited at the initial (I_o) and intermediate (I) positions along the fibre as a function of distance. The red lines in the right graphs stand for fits to exponential laws of **NI1** (λ_{exc} = 355 nm).

Stimuli-responsive fluorochromism

We have found that the solid-state emission properties of both compounds can be modulated in response to temperature. Specifically, the fluorescence of thin films prepared by blade-coating of **NI1** and **NI2** (with thicknesses of 280 and 380 nm respectively as determined by optical profilometry) varied when they were heated above 140 °C and 100 °C, respectively. Fig. 4c and d show photographs of the as-prepared thin films of **NI1** and **NI2**, respectively, visualized under a UV lamp (365 nm) before and after annealing showing the heat-induced colour switch. Interestingly the original emission colour can be restored in both films upon grinding with a spatula. Fluorescence spectra of the emissive layers after thermal treatment confirmed that in both cases the PL spectrum blueshifts from 649 nm to 605 nm in **NI1** and from 585 to 566 nm in **NI2** (Fig. 4a and b), and confirmed that in both cases, upon subsequent shearing at the emission wavelength it is recovered, returning to the starting point. Absorption and excitation spectra of the samples before and after heating do not show significant changes in the two cases (Fig. S10, ESI†).

Powder X-ray diffraction was conducted to understand the phase transitions leading to the colour change. For both compounds, initial amorphous thin layers were observed (Fig. 5). After heating, a crystallization phase transition is evidenced by the presence of sharp and intense reflection peaks in the X-ray diffractogram, suggesting that the colour change observed corresponds to a change between an amorphous-phase and a crystalline phase. Upon shear-induced amorphization, molecules may experience an increase in rotational freedom facilitating their rearrangement to form new intermolecular charge-transfer species or excimers.[48] Note that flat NI moieties have a strong tendency to form excimers due to associative interactions between excited and ground state molecules, which could be responsible for the emission red shift in amorphous **NI1** and **NI2**.[49,50]

Differential scanning calorimetry (DSC) results further confirmed that a cold-crystallization is taking place when both compounds are heated (Fig. 6 and Fig. S13, ESI†).[51,52] As illustrated in Fig. 6, in the first heating cycle, **NI2** shows a glass

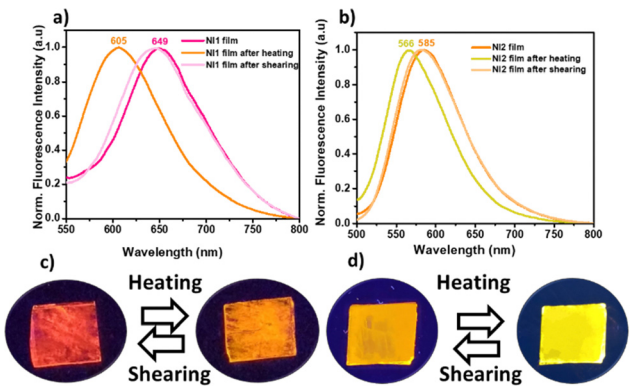

Fig. 4 Fluorescence spectrum of the thin films of (a) **NI1** and (b) **NI2** as obtained by blade-coating, after heating and after subsequent shearing to return to the initial colour. Photographs of thin film layers illuminated with a 365 nm UV lamp under the different stimuli for (c) **NI1** and (d) **NI2**.

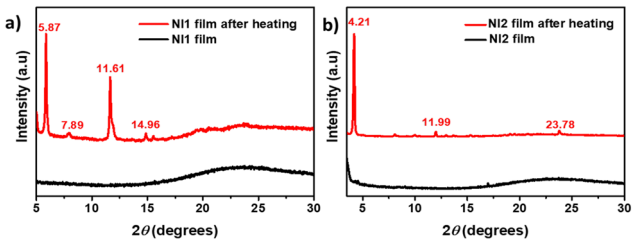

Fig. 5 Powder X-ray diffraction pattern for (a) **NI1** and (b) **NI2** in pristine films and after heating.

transition at 32.5 °C, followed by a cold-crystallization transition peak at 102.4 °C (4.76 kJ mol^{-1}). The sharp endothermic peak at 127.5 °C corresponds to the melting of the crystalline phase. In the cooling cycle, we only observed a glass transition. **NI1** also shows a cold-crystallization at 137.3 °C (1.15 kJ mol^{-1}) before melting at 174.6 °C (Fig. S13, ESI†). A similar thermal behaviour is observed in the second DSC cycle highlighting the reversibility of the process (Fig. S14, ESI†). Thermogravimetric analysis (TGA) shows good thermal stability of both compounds in the range of the phase transition (Fig. S15, ESI†).

X-Ray structure determination

In order to shed light on how crystallization influences the colour emission of these two compounds, we determined the structural packing in the crystals by single crystal X-ray analysis (see ESI,† Section S7). Compound **NI1** crystallized in the *P*21 space group with two independent molecules in the asymmetric unit (Fig. 7a). The needle-shaped crystals were extremely small in two of the three dimensions and formed sheaf-like aggregates. Many attempts were made to grow better crystals, and ultimately the best available fragment (among numerous crystals tested) was selected for the diffraction experiment; however, the resulting diffraction pattern shows the existence of peaks belonging to small domains that could not be segregated at the integration phase. The two **NI1** molecules that form the dimer differ in the torsion angle between the phenyl ring of the triphenylamine on one side of the alkyne and the naphthalimide moiety which are nearly coplanar (2(2)° and 7(2)°) as well

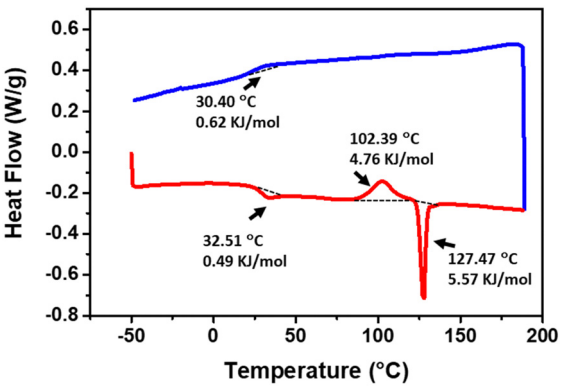

Fig. 6 DSC curves for heating (red) and cooling (blue) of **NI2** measured at 10 °C min^{-1}. Exo up.

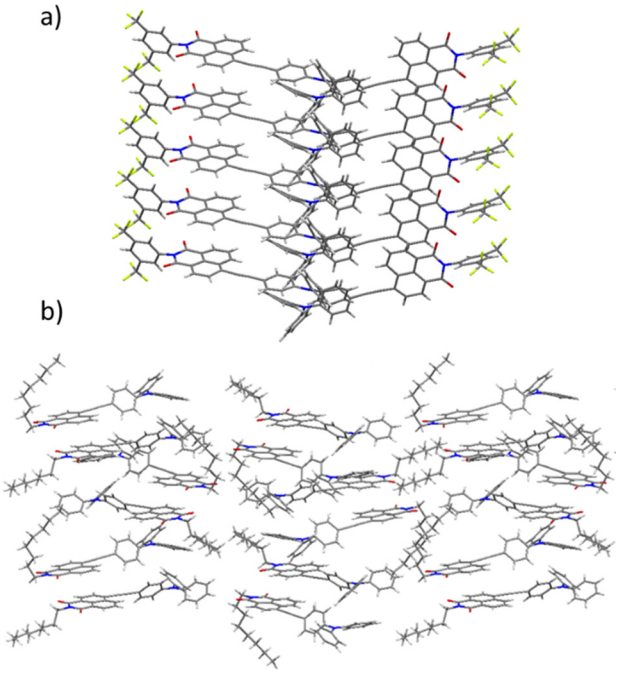

Fig. 7 Lateral view of the dimers and columns that emerge as a result of the crystallographic packing of molecules of (a) **NI1** and (b) **NI2**.

as in the torsion of the attached diCF$_3$-phenyl groups (80(2)° and 74(2)°) (Fig. 8a).

On the other hand, compound **NI2** crystallizes in the *P*21/*n* space group with two independent molecules in the asymmetric unit (Fig. 7b). In this case, we again observe differences in the torsion angle of the phenyl ring of the triphenylamine and the naphthalimide moiety (which exhibit values much larger than in the previous case, 58.2(3)° and 42.9(4)°), as well as in the disposition of the long alkyl chains, one of them nearly orthogonal to the NI moiety, introducing a high steric hindrance (Fig. 8b).

An analysis of the crystallographic packing shows that the two independent molecules of **NI1** organize into two different columns that grow along the b axis. Such an arrangement results in extended stacks of the NI moieties, which are laterally shifted by approximately 43°. This type of aggregate is highly desirable for light transport and photonic applications.[53] In contrast, the two crystallographically independent molecules of **NI2** organize to form dimers with the NI moieties laterally shifted by around 38° giving rise to an arrangement in which lateral alkyl chains remain interdigitated along the whole structure. Examining the close contacts between adjacent molecules reveals that both structures are stabilized by multiple CH–π and π–π interactions involving the triphenylamine, alkyne groups and NI moiety of neighbouring molecules. Significantly shorter contact distances are observed between **NI2** molecules when compared to **NI1**, pointing to stronger intermolecular interactions, thus explaining the higher transition phase enthalpies recorded for **NI2** (4.76 kJ mol^{-1} *vs.* 1.07 kJ mol^{-1}).

Interestingly, in both cases the powder X-ray diffractograms simulated from the single-crystal data coincide with those obtained from the crystallized films (Fig. S21, ESI†). Note that

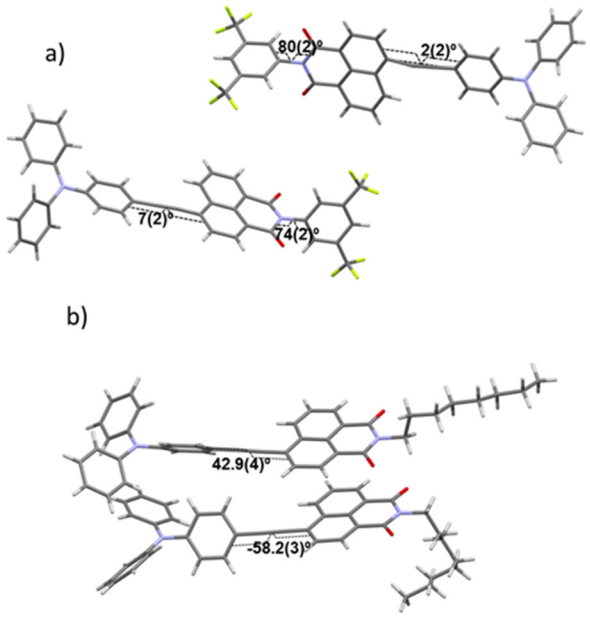

Fig. 8 View of the two independent molecules in the asymmetric unit of (a) **NI1** and (b) **NI2**.

meniscus-guided processing techniques, such as blade-coating, favour highly aligned films, and therefore, only the most intense peaks are observed.[54] This good match allowed us to investigate the origin of the colour changes between the two interconverted phases induced by a thermal or mechanical stimulus. Presumably, during shear-induced amorphization, the distance between the highly emissive NI molecules is reduced, thus promoting intermolecular electronic delocalization. In the case of **NI1**, the presence of more extended stacks together with the possible planarization of the highly distorted diCF_3-phenyl substituents (thus resulting also in an intramolecular contribution to the colour change) is probably responsible for the larger bathochromic shift in this particular case. In contrast, in **NI2**, where a dimeric packing arrangement is induced due to steric hindrance introduced by the flexible chains, the colour change is notably less pronounced.

Conclusions

In this work, we have synthetized two D–π–A NI derivatives, with different functionalities in the NI core (diCF_3-phenyl or octyl chains) following the principles of sustainable chemistry by employing microwave irradiation as the energy source, a minimal amount of solvent and a reusable catalyst. Both compounds self-assemble by slow diffusion and led to the formation of single crystals suitable for XRD analysis. The presence of a diCF_3-phenyl group is beneficial to obtain larger crystals when compared to the alkyl chains. The waveguiding behaviour of both compounds was confirmed by PL microscopy and the optical loss coefficient for **NI1** was measured, being lower than previously reported ones.

Both compounds are strongly fluorescent and present a reversible stimuli-responsive behaviour under thermal and mechanical action. An amorphous-to-crystalline phase transition is induced by heating (cold crystallization), giving rise to a blue shift of the emission colour that can be reverted due to an amorphization process upon shearing.

X-ray analysis of the crystalline packing shows different arrangements for these compounds in which N-substitution plays a crucial role in the final structure.

The combination of the properties of these crystalline organic waveguides with the thermal/mechanical reversible stimuli-responsiveness, may lead to broad applications such as in tunable optics, security inks or rewritable materials.

We hope that these findings will provide important structural clues for the *ad hoc* design of smart materials with desired properties and functions.

Author contributions

R. Martín: investigation, methodology, data curation, interpretation, writing – review and editing. A. Sánchez-Oliva: investigation, methodology, data curation. A. Benito: investigation, methodology, data curation, analysis and interpretation of results. I Torres-Moya: investigation, supervision, data curation. A. M. García: methodology, data curation, writing the original draft. J. Álvarez-Conde: investigation, data curation. J. Cabanillas-González: investigation, data curation, funding acquisition, supervision. P. Prieto: conceptualization, supervision; funding acquisition, writing – review and editing. B. Gómez-Lor: conceptualization, supervision; interpretation, funding acquisition, writing – review and editing. All authors reviewed the results and approved the final version of the manuscript.

Conflicts of interest

There are no conflicts to declare.

Acknowledgements

This research was funded by MCIN/AEI/10.13039/501100011033 (Projects PID2019-104125RB-I00, PID2020-119636GB-I00, PDC2021-121002-I00 and PID2021-128313OB-I00), by FEDER and Junta de Comunidades de Castilla-La Mancha (JCCM-FEDER) (Project SBPLY/21/180501/000114) and by the Regional Government of Madrid (NMAT2D-CM). A. Sánchez-Oliva acknowledges the Universidad de Castilla-La Mancha (UCLM) for a predoctoral grant for Personal Investigador en Formación (2021-UNIVERS-10626), funded by the Fondo Social Europeo Plus (FSE +). I. Torres-Moya acknowledges the Agencia Estatal de Investigación for a post-doctoral grant Juan de la Cierva Formación 2020 FJC2020-043684-I funded by MCIN/AEI/10.13039/501100011033 and European Union NextGeneration EU/PRTR. A. M. Garcia acknowledges the María Zambrano program under the grant agreement UNI/551/2021. R. Martín acknowledges the Spanish Ministry of Universities for a Margarita Salas postdoctoral fellowship under the agreement UNI/551/2021. J. Cabanillas-González also acknowledges a Research

Consolidation Grant (CNS2022-136191) from the Spanish Ministry of Science and Innovation. IMDEA Nanociencia acknowledges support from the 'Severo Ochoa' Programme for Centres of Excellence in R&D of the Spanish Ministry of Science and Innovation (CEX2020-001039-S). We also thank J. Perles, M. Ramirez and P. Martínez for their collaboration in solving the crystal structure of NIs.

References

1 L. Tong, R. R. Gattass, J. B. Ashcom, S. He, J. Lou, M. Shen, I. Maxwell and E. Mazur, *Nature*, 2003, **426**, 816–819.
2 Q. H. Cui, Y. S. Zhao and J. Yao, *J. Mater. Chem.*, 2012, **22**, 4136–4140.
3 H. Jiang and W. Hu, *Angew. Chem., Int. Ed.*, 2020, **59**, 1408–1428.
4 D. Tian and Y. Chen, *Adv. Opt. Mater.*, 2021, 2002264.
5 S. Wu, B. Zhou and D. Yan, *Adv. Opt. Mater.*, 2021, 2001768.
6 S. Chen, M.-P. Zhuo, X.-D. Wang, G.-Q. Wei and L.-S. Liao, *PhotoniX*, 2021, **2**, 2.
7 Y. Shi and X. Wang, *Adv. Funct. Mater.*, 2021, **31**, 2008149.
8 C. Zhang, J. Y. Zheng, Y. S. Zhao and J. Yao, *Adv. Mater.*, 2011, **23**, 1380–1384.
9 M. Zhuo, Y. Su, Y. Qu, S. Chen, G. He, Y. Yuan, H. Liu, Y. Tao, X. Wang and L. Liao, *Adv. Mater.*, 2021, **33**, 2102719.
10 Q. Di, L. Li, X. Miao, L. Lan, X. Yu, B. Liu, Y. Yi, P. Naumov and H. Zhang, *Nat. Commun.*, 2022, **13**, 5280.
11 R. Chandrasekar, *Chem. Commun.*, 2022, **58**, 3415–3428.
12 X. Yang, L. Lan, X. Pan, X. Liu, Y. Song, X. Yang, Q. Dong, L. Li, P. Naumov and H. Zhang, *Nat. Commun.*, 2022, **13**, 7874.
13 M. Annadhasan, S. Basak, N. Chandrasekhar and R. Chandrasekar, *Adv. Opt. Mater.*, 2020, **8**, 2000959.
14 Z. Ding, H. Shang, Y. Geng, S.-T. Zhang, Z. Huo, Z. Yang, B. Li, W. Xu and S. Jiang, *J. Phys. Chem. Lett.*, 2021, **12**, 4585–4592.
15 N. Mitetelo, D. Venkatakrishnarao, J. Ravi, M. Popov, E. Mamonov, T. V. Murzina and R. Chandrasekar, *Adv. Opt. Mater.*, 2019, **7**, 1801775.
16 J. Mahmoud Halabi, E. Ahmed, S. Sofela and P. Naumov, *Proc. Natl. Acad. Sci. U. S. A.*, 2021, **118**, e2020604118.
17 S. Yousuf, J. Mahmoud Halabi, I. Tahir, E. Ahmed, R. Rezgui, L. Li, P. Laws, M. Daqaq and P. Naumov, *Angew. Chem., Int. Ed.*, 2023, **62**, e202217329.
18 Y. Ma, Y. Li, L. Chen, Y. Xiong and G. Yin, *Dyes Pigm.*, 2016, **126**, 194–201.
19 Y. Li, Z. Ma, A. Li, W. Xu, Y. Wang, H. Jiang, K. Wang, Y. Zhao and X. Jia, *ACS Appl. Mater. Interfaces*, 2017, **9**, 8910–8918.
20 C. Feng, K. Wang, Y. Xu, L. Liu, B. Zou and P. Lu, *Chem. Commun.*, 2016, **52**, 3836–3839.
21 P. Galer, R. C. Korošec, M. Vidmar and B. Šket, *J. Am. Chem. Soc.*, 2014, **136**, 7383–7394.
22 J. Feng, K. Tian, D. Hu, S. Wang, S. Li, Y. Zeng, Y. Li and G. Yang, *Angew. Chem., Int. Ed.*, 2011, **50**, 8072–8076.
23 D. Genovese, A. Aliprandi, E. A. Prasetyanto, M. Mauro, M. Hirtz, H. Fuchs, Y. Fujita, H. Uji-I, S. Lebedkin, M. Kappes and L. De Cola, *Adv. Funct. Mater.*, 2016, **26**, 5271–5278.
24 X. Wang, W. Li, W. Li, C. Gu, H. Zheng, Y. Wang, Y.-M. Zhang, M. Li and S. Xiao-An Zhang, *Chem. Commun.*, 2017, **53**, 11209–11212.
25 M. I. Khazi, W. Jeong and J. Kim, *Adv. Mater.*, 2018, **30**, 1705310.
26 M.-J. Teng, X.-R. Jia, S. Yang, X.-F. Chen and Y. Wei, *Adv. Mater.*, 2012, **24**, 1255–1261.
27 C. Wang and Z. Li, *Mater. Chem. Front.*, 2017, **1**, 2174–2194.
28 D. Wang, X. Zhang, X. Han, Y. Zhou, Y. Lei, W. Gao, M. Liu, X. Huang and H. Wu, *J. Mater. Chem. C*, 2021, **9**, 12868–12876.
29 M. Echeverri, C. Ruiz, S. Gámez-Valenzuela, I. Martín, M. C. Ruiz Delgado, E. Gutiérrez-Puebla, M. Á. Monge, L. M. Aguirre-Díaz and B. Gómez-Lor, *J. Am. Chem. Soc.*, 2020, **142**, 17147–17155.
30 Z.-D. Yu, X.-X. Dong, J.-Y. Cao, W.-X. Zhao, G.-H. Bi, C.-Z. Wang, T. Zhang, S. Rahman, P. E. Georghiou, J.-B. Lin and T. Yamato, *J. Mater. Chem. C*, 2022, **10**, 9310–9318.
31 B. Prusti, P. Sarkar, S. K. Pati and M. Chakravarty, *J. Mater. Chem. C*, 2021, **9**, 9555–9570.
32 M. Echeverri, C. Ruiz, S. Gámez-Valenzuela, M. Alonso-Navarro, E. Gutierrez-Puebla, J. L. Serrano, M. C. Ruiz Delgado and B. Gómez-Lor, *ACS Appl. Mater. Interfaces*, 2020, **12**, 10929–10937.
33 H. Park, I. E. Serdiuk and S. Y. Park, *ChemPhotoChem*, 2023, **7**, e202200267.
34 I. Torres-Moya, J. R. Carrillo, M. V. Gómez, A. H. Velders, B. Donoso, A. M. Rodríguez, Á. Díaz-Ortiz, J. T. López Navarrete, R. P. Ortiz and P. Prieto, *Dyes Pigm.*, 2021, **191**, 109358.
35 M. Poddar, G. Sivakumar and R. Misra, *J. Mater. Chem. C*, 2019, **7**, 14798–14815.
36 D. Wu, A. C. Sedgwick, T. Gunnlaugsson, E. U. Akkaya, J. Yoon and T. D. James, *Chem. Soc. Rev.*, 2017, **46**, 7105–7123.
37 S. Banerjee, E. B. Veale, C. M. Phelan, S. A. Murphy, G. M. Tocci, L. J. Gillespie, D. O. Frimannsson, J. M. Kelly and T. Gunnlaugsson, *Chem. Soc. Rev.*, 2013, **42**, 1601.
38 R. Martín, P. Prieto, J. R. Carrillo, A. M. Rodríguez, A. de Cozar, P. G. Boj, M. A. Díaz-García and M. G. Ramírez, *J. Mater. Chem. C*, 2019, **7**, 9996–10007.
39 J. W. Chung, Y. You, H. S. Huh, B.-K. An, S.-J. Yoon, S. H. Kim, S. W. Lee and S. Y. Park, *J. Am. Chem. Soc.*, 2009, **131**, 8163–8172.
40 K. Kümmerer, *Angew. Chem., Int. Ed.*, 2017, **56**, 16420–16421.
41 P. T. Anastas and J. C. Warner, *Green Chemistry: Theory and Practice*, Oxford University Press, 1998.
42 Z. Lu, Y. Zhang, H. Liu, K. Ye, W. Liu and H. Zhang, *Angew. Chem., Int. Ed.*, 2020, **59**, 4299–4303.
43 V. Vinay Pradeep, C. Tardío, I. Torres-Moya, A. M. Rodríguez, A. Vinod Kumar, M. Annadhasan, A. Hoz, P. Prieto and R. Chandrasekar, *Small*, 2021, **17**, 2006795.
44 H. Liu, Z. Lu, Z. Zhang, Y. Wang and H. Zhang, *Angew. Chem., Int. Ed.*, 2018, **57**, 8448–8452.

45 C. Tardío, J. Álvarez-Conde, I. Torres-Moya, A. M. Rodríguez, A. De La Hoz, J. Cabanillas-González and P. Prieto, *J. Mater. Chem. C*, 2022, **10**, 6411–6418.
46 M. Annadhasan, D. P. Karothu, R. Chinnasamy, L. Catalano, E. Ahmed, S. Ghosh, P. Naumov and R. Chandrasekar, *Angew. Chem., Int. Ed.*, 2020, **59**, 13821–13830.
47 C. Zhang, C.-L. Zou, Y. Yan, R. Hao, F.-W. Sun, Z.-F. Han, Y. S. Zhao and J. Yao, *J. Am. Chem. Soc.*, 2011, **133**, 7276–7279.
48 S. Varughese, *J. Mater. Chem. C*, 2014, **2**, 3499.
49 D. W. Cho and D. W. Cho, *New J. Chem.*, 2014, **38**, 2233–2236.
50 D. W. Cho, M. Fujitsuka, K. H. Choi, M. J. Park, U. C. Yoon and T. Majima, *J. Phys. Chem. B*, 2006, **110**, 4576–4582.
51 Y. Tsujimoto, T. Sakurai, Y. Ono, S. Nagano and S. Seki, *J. Phys. Chem. B*, 2019, **123**, 8325–8332.
52 W. R. Bodlos, S. Mattiello, A. Perinot, L. Gigli, N. Demitri, L. Beverina, M. Caironi and R. Resel, *Cryst. Growth Des.*, 2021, **21**, 325–332.
53 P. Lova, V. Grande, G. Manfredi, M. Patrini, S. Herbst, F. Würthner and D. Comoretto, *Adv. Opt. Mater.*, 2017, **5**, 1700523.
54 X. Gu, L. Shaw, K. Gu, M. F. Toney and Z. Bao, *Nat. Commun.*, 2018, **9**, 534.